Ultrahigh-Gain Single SnO_2 Microrod Photoconductor on Flexible Substrate with Fast Recovery Speed

Kewei Liu, Makoto Sakurai, Masakazu Aono, and Dezhen Shen*

Owing to the special properties and wide applications, UV photodetectors based on wide-band-gap semiconductors have drawn an increasing interest during the last two decades. However, practical UV photodetectors are required two contradictory performances: high internal gain and fast recovery speed, because high internal gain is achieved by long life time of photoexcited carriers and fast recovery needs their fast decay. Their slow decay in wide-band-gap semiconductors has been known as a persistent photoconductivity (PPC) problem and hinders applications. In this paper, a good solution to the above contradictory problem is demonstrated on a single SnO_2 microrod photoconductor, which shows both high photoconductive gain ($\approx 1.5 \times 10^9$) and quick recovery speed (<1 s). Notably, the quick recovery speed is associated with the removal of the persistent photoconductivity effect (>1 d), which is induced by a novel "reset" process: bending and straightening the microrod and subsequently applying a voltage pulse. This result suggests that SnO_2 microrods have potential applications in high-performance UV photodetecting devices.

1. Introduction

UV photodetectors have attracted considerable attention due to their effective applications in the fields of missile early warning, wireless communication, flame sensing, environmental monitoring, space research, and medical treatment.[1–4] Until now, various types of UV photodetectors have been realized including p–n junction, Schottky barrier photodiodes, and photoconductors.[5–8] In particular, owing to their high photo-responsivity from photoconductive gain, simple fabrication process, and low cost, UV photoconductors offer an attractive alternative for low-light detection without any preamplifier, and achieved widely commercial applications.[9,10] Unfortunately, UV photoconductors are not without their disadvantages. As is well known, the internal photoconductive gain is induced by the trapping of minority carriers on the defects. Thus, the large photoconductive gain is usually accompanied by slow recovery speed due to the persistent photoconductivity (PPC) effect,[11–13] which means that the UV photoconductors are difficult to detect the change of light intensity at high frequency. In order to solve this contradiction and fabricate the photoconductor with high responsivity and high speed, it is necessary to control the PPC effect rapidly, dynamically, and intentionally. Until now, there have been many approaches to achieving this purpose, such as the application of electric field or light pulses, and the employment of three-terminal device structure, and so on.[14–17] However, the application of electric field or light pulses in a two-terminal device usually could not completely remove the PPC effect, and the control speed is also not very quick.[14,16,17] Although the PPC effect can be erased rapidly and completely by applying the gate voltage in three-terminal devices, they are structurally complex.[15] Therefore, to realize a simple photoconductor with high internal gain and fast recovery, the effective method, which can control the PPC effect rapidly, dynamically, and intentionally, is urgently required.

Due to its excellent electrical, chemical, and optoelectronic properties, SnO_2 has been widely used as transparent conductors, chemical sensors, and photodetectors.[18–22] In particular, SnO_2-based photoconductors usually have a large internal gain, but their recovery speed is relatively slow due to the PPC effect as aforementioned.[19,23–27] Thus, SnO_2 can serve as an ideal model system to investigate the manipulation of the PPC effect. Very recently, we have demonstrated that the mechanical strain-induced defects can trap the free electrons in SnO_2, causing the transition from the semiconducting state to the insulating state.[28,29] By applying an appropriate voltage, the defects are electrically healed and the insulating state reverts to the original semiconducting state. This reversible trap and release of free electrons controlled by stress and voltage could be a potential method for removing the excess electrons and, in turn, for eliminating the PPC effect. Thus, a high-performance SnO_2 UV photoconductor is expected to be realized with both high responsivity and quick response speed.

Motivated by the above-mentioned results and predictions, here we demonstrate a single SnO_2 microrod photoconductor on a flexible Kapton substrate. The responsivity of the device

Prof. K. Liu, Prof. D. Shen
State Key Laboratory of Luminescence and Applications
Changchun Institute of Optics
Fine Mechanics and Physics (CIOMP)
Chinese Academy of Sciences (CAS)
Changchun 130033, P. R. China
E-mail: Liukw@ciomp.ac.cn
Prof. M. Sakurai, Prof. M. Aono
International Center for Materials Nanoarchitectonics (MANA)
National Institute for Materials Science (NIMS)
Tsukuba 305-0044, Japan

DOI: 10.1002/adfm.201500231

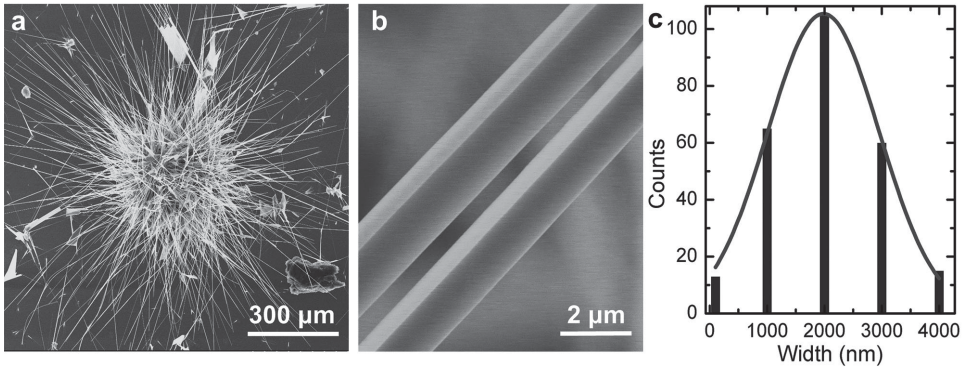

Figure 1. a,b) SEM images of as-grown SnO_2 microrods. c) Statistical side-width distribution of SnO_2 microrods, and the corresponding Gaussian fitting curve.

can reach as high as $\approx 3 \times 10^8$ A W^{-1}, corresponding to an internal gain of $\approx 1.5 \times 10^9$ A W^{-1} due to the PPC effect (photoconductivity can persistent for more than 20 h after the light is switched off). More interestingly, this giant PPC in SnO_2 microrods can be eliminated by a novel reset process: bending–straightening the microrod and subsequently applying an appropriate voltage. The mechanisms of PPC and its elimination have been investigated in detail. Our findings may pave a new way for fabricating high-performance photoconductors.

2. Results and Discussion

Figure 1a,b shows the typical scanning electron microscope (SEM) images of the as-grown SnO_2 microrods on the Si substrate. The microrods are well faceted and have square cross sections with the length of 0.5–1.5 mm. (The length can even reach as long as 8 mm in some place.) The cross-section widths of square show a narrow distribution and the average width is around 1–3 μm as shown in Figure 1c. Energy-dispersive X-ray spectroscopy (EDX) line profile analysis was performed across the width of SnO_2 microrod (see **Figure 2**a). The line-scan profiles of O and Sn show a similar rectangular shape, indicating the uniformity of the distribution of Sn and O within each individual microrod. Figure 2b presents the X-ray diffraction (XRD) patterns from a single microrod. When the scattering vector q is parallel to the rod axis, the diffraction peaks at $2\theta = 25.8°$, 52.9°, and 83.7° can be assigned to (002), (004), and (006) orientations of rutile SnO_2, respectively (see the top of Figure 2b). Once q is parallel to the diagonal line of square cross-section

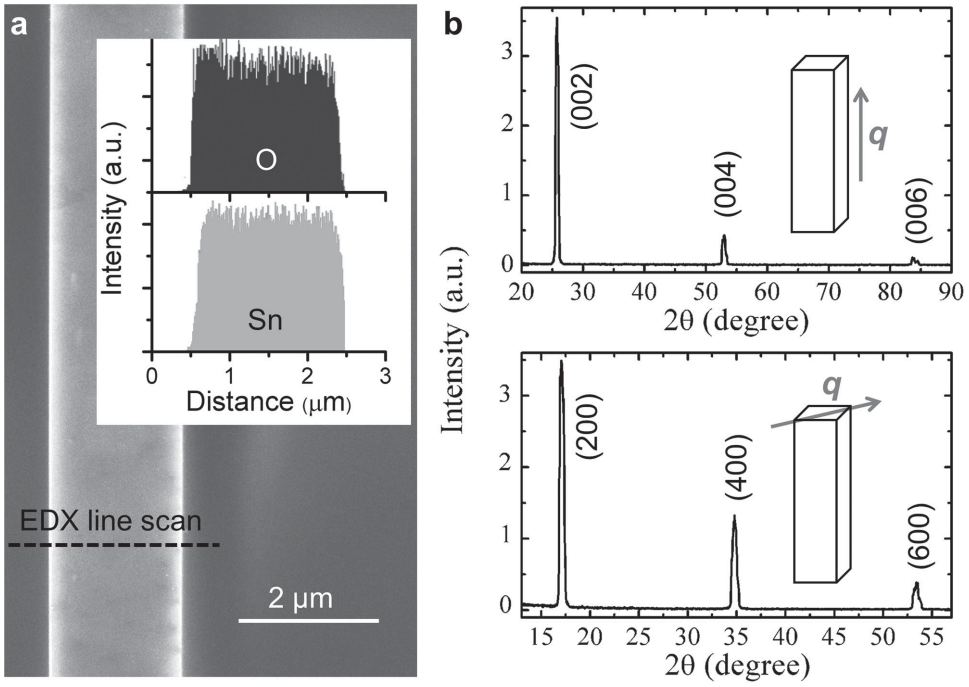

Figure 2. a) SEM image of a SnO_2 microrod and the corresponding EDX line scan profile across the rod (the dot line). XRD patterns of as-grown single SnO_2 microrod, b) scattering vector q parallel to rod axis, and c) scattering vector q parallel to the diagonal line of square cross-section of SnO_2 microrod.

of SnO_2 microrod, (200), (400), and (600) diffraction peaks can be observed at $2\theta = 17.1°$, 34.8°, and 53.4°, respectively (see the bottom of Figure 2b). The XRD results suggest that the SnO_2 microrods possess a single-crystal rutile structure with the growth direction along the [001] axis and they are enclosed by the (110) facets. The lattice constant of rutile SnO_2 can be calculated as $a = 0.478$ nm and $c = 0.318$ nm. In order to get a further insight into the structure of the SnO_2 microrod, the high-resolution transmission electron microscopy (HRTEM) measurement was carried out on an individual SnO_2 nanorod, which is co-fabricated with microrod at the same substrate. **Figure 3** shows the HRTEM image and microstructure of the sample. The distance between two adjacent lattice fringes parallel and perpendicular to the microrod axis is found to be 0.34 nm and 0.32 nm, and these planes can be indexed as (110) and (001) of rutile SnO_2. The HRTEM results are in excellent agreement with the XRD results.

A schematic illustration of a SnO_2 single microrod device for the measurement of the photoconducting properties is shown in the inset in **Figure 4**a. An individual SnO_2 microrod was placed on the Kapton substrate and the two ends of the microrod were tightly fixed by 500 nm thick Au electrodes. The distance between the inner edges of two Au electrodes is ≈300 μm. The current–voltage (I–V) curve of the device in dark at room temperature (23 °C) is presented in Figure 4a. The linear I–V curve indicates the formation of ohmic contacts between the Au electrodes and the microrod. Thus, the resistivity of SnO_2 microrod can be calculated to be around 0.1 Ω cm at 23 °C from the I–V curve. According to the previous reports, SnO_2 is a typical n-type semiconductor due to its intrinsic impurities, such as oxygen vacancies.[21] Figure 4b shows the the logarithm of the resistance R ($\ln R$) as a function of inverse temperature (Arrhenius plot). Experimental data can be well fitted by the following equation

$$R = Ae^{\frac{E_a}{k_B T}} \quad (1)$$

where A denotes a material parameter, which does not depend on temperature, E_a is the activation energy, and k_B is the Boltzmann constant. The activation energy E_a determined from the slope of resistance data in Figure 4b is around 69 meV. This value is in well agreement with that reported previously.[30]

Figure 5a shows the photocurrent rise upon continuous UV light illumination (λ = 260 nm) and the photocurrent decay after the removal of incident light under different conditions at a 2 V bias. Upon exposure to 260 nm illumination, a short rapid photocurrent increase is observed, followed by a slow increase for all different conditions. After turning off the light, the photocurrent shows an ultra-slow decay, and the estimated characteristic recovery time is of the order of days as shown in Figure 5a. By comparing the curves at 23 °C and 58 °C in air, it is found that the decay time of the photoinduced conductivity depends on temperature and becomes longer with decreasing temperature. Moreover, at a fixed temperature of 23 °C, the photocurrent decay in air is faster than that in vacuum. The results in Figure 5a are consistent with the previous reports, and the oxygen vacancy both on the surface and in the bulk is a possible candidate responsible for the giant PPC in SnO_2

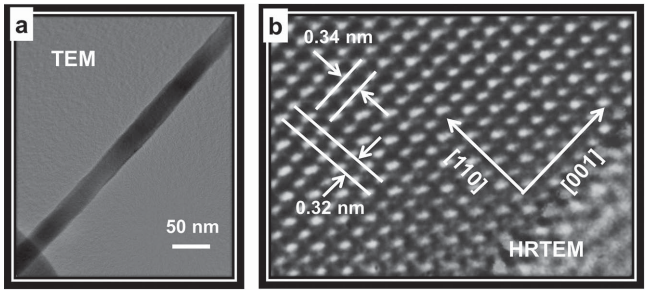

Figure 3. a) TEM image of a single as-grown SnO_2 nanorod. b) High-resolution TEM image of SnO_2 nanorod.

microrod.[27] The decay of the photoinduced conductivity at a fixed temperature does not follow a simple exponential law. Usually, the PPC decay could be described by the stretched exponential function[31]

$$I_{PPC}(t) = I_{PPC}(0)e^{-(t/\tau)^{\beta}} \quad (2)$$

where $I_{PPC}(0)$ is defined as the PPC buildup level at the moment of light illumination being removed, τ is the PPC decay time

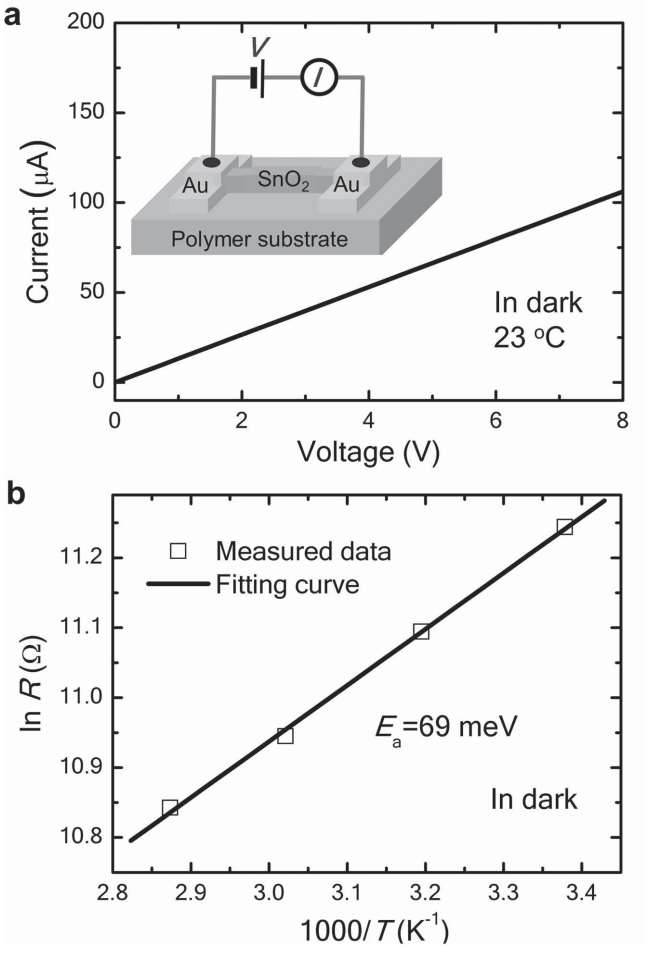

Figure 4. a) Dark current–voltage of the SnO_2 single microrod photoconductor at 23 °C. The inset is the schematic illustration of the device. b) Arrhenius plots of ln$R$ versus the inverse temperature.

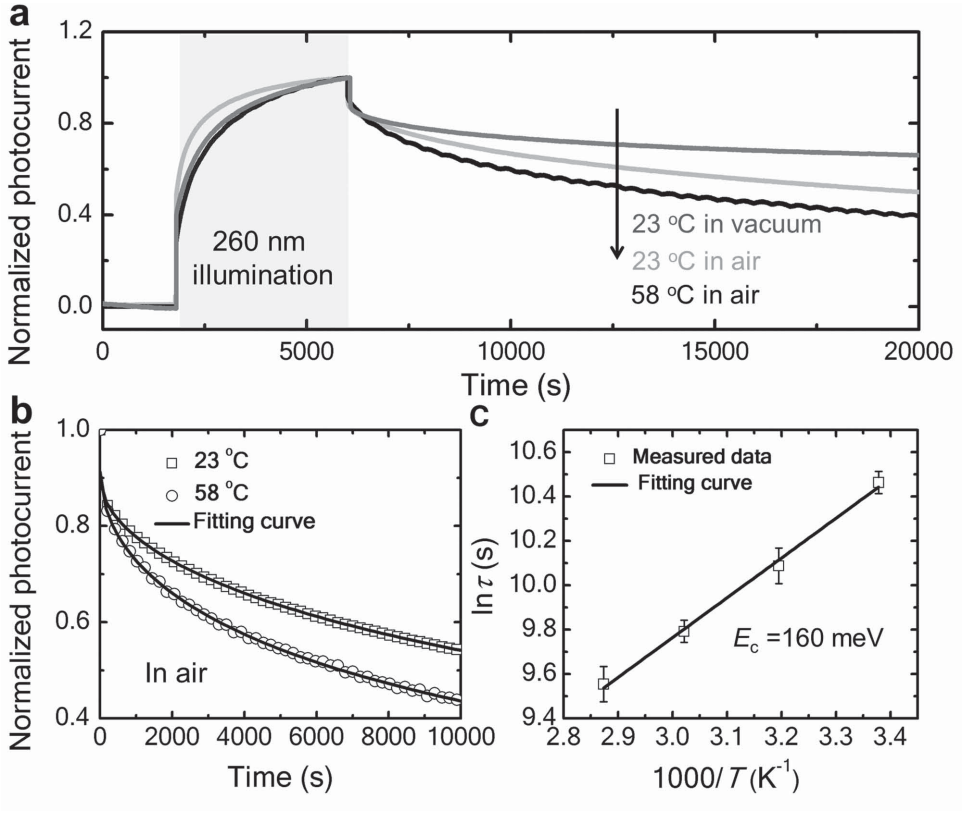

Figure 5. a) Typical PPC behavior in SnO_2 single microrod irradiated by 260 nm UV light with 2 V applied voltage under different conditions: 23 °C in vacuum, 23 °C in air, and 58 °C in air. The excitation intensity is around 0.05 μW cm^{-2}. b) The normalized photocurrent decay in air at 23 °C (open square) and 58 °C (open circle). The PPC decay time constants are determined by fitting the decay curves using the stretched-exponential equation. c) Arrhenius plot of the PPC decay time constant as a function of the inverse temperature. The hole capture barrier is determined to be 160 meV.

constant, and β is the decay exponent ($0 < \beta < 1$). Figure 5b shows PPC decay at 23 °C and 58 °C in air. The experimental data are better fitted with Equation (2). The fitted values of β are between 0.51 and 0.54 and are not significantly affected by temperature in the studied temperature range (20–80 °C). Figure 5c shows the Arrhenius plot of the fitted time constants of the SnO_2 microrods. In the measured temperature range, τ exhibits a thermally activated behavior described by the following function[31]

$$\tau = \tau_0 e^{\frac{E_c}{k_B T}} \quad (3)$$

where E_c is the hole capture barrier determined to be 160 meV using a linear fit. We attribute the PPC primarily to the subgap and surface traps of the SnO_2 microrod. The contribution of the surface traps becomes larger with the increase of the surface-to-volume ratio, as observed in the SnO_2 nanobelt device.[27]

The ultra-slow decay of photocurrent in SnO_2 microrod hinders its applications as UV photodetectors, although it is also associated with the large internal photoelectric gain. Thus, to realize the photoconductors with both fast recovery speed and large internal gain, the elimination of the PPC effect is required after the removal of incident light. According to our previous results,[28,29] the conductance of SnO_2 microrod in dark could be controlled by introducing the strain and applying the voltage. This novel process is thus expected to be used to estimate the PPC effect and increase the decay speed of photocurrent in SnO_2 microrod. **Figure 6** shows the response characteristics of the photoconductance of SnO_2 microrod to the 260 nm light illumination (≈0.05 μW cm^{-2}) under the bias of 2 V. The variation of the ratio of UV-exposed current to dark current for SnO_2 microrod was ≈170%. The dark current and UV-exposed current of the SnO_2 microrod were around 26 μA and 44 μA, respectively. After turning off the light, the giant PPC effect can be observed in SnO_2 microrod. Interestingly, when we bend the microrod (the tensile strain $\varepsilon = 0.15\%$, and the calculation method was shown in Figure S1 in the Supporting Information) and subsequently release it, the current decreased abruptly to a very low value (below the instrumental limit). After the application of 8 V bias, the current increased rapidly. As a result, the current returned to close to the initial dark value, and the PPC effect was effectively eliminated by this novel "reset" process (see the inset of Figure 6 and Figure S2 in the Supporting Information). Thus, the recovery time of SnO_2 microrod photoconductor can be reduced to below 1 s by the "reset" process, which is shorter than that of the conventional SnO_2 photodetectors (see **Table 1**). This phenomenon can be explained as follows: first, the electron–hole pairs are excited in SnO_2 microrod by UV light, and holes are readily trapped at the deep level defects, leaving behind unpaired electrons. After light illumination, the minority carrier trapping effect limits the recombination process, which produces the giant PPC. When

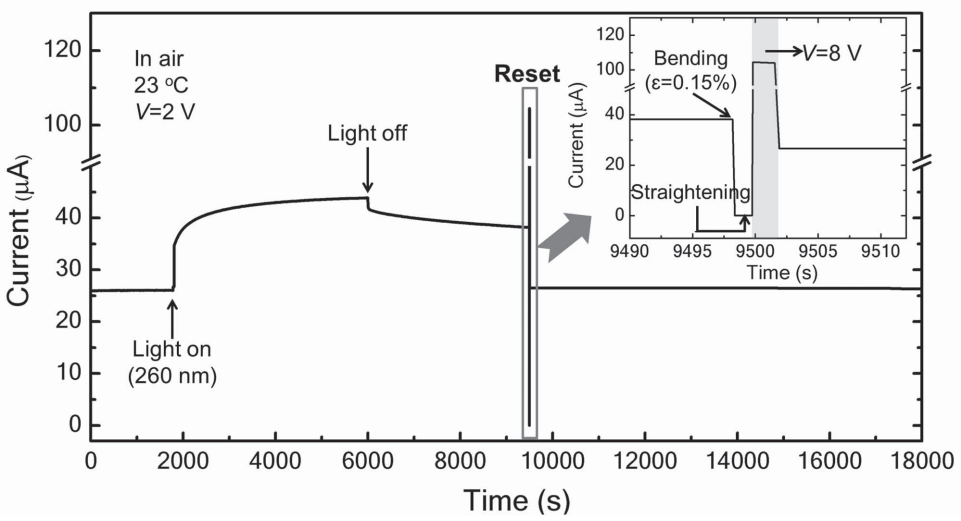

Figure 6. The time-dependent photoresponse of the SnO_2 single microrod photodetector to UV illumination at 23 °C, and the photocurrent decay rate can be significationally increased by a novel "reset" process: bending–straitening–pulse voltage application (inset).

we bend the microrod, the slip planes are formed in SnO_2 microrod under tensile strain, and the lattice defects tend to be created on the slip plane and to be distributed locally about the plane according to our previous result.[29] These lattice defects can trap free electrons, inducing the significant decrease in the conductance of SnO_2 microrod. Moreover, the lattice defects could also act as the recombination centers of the photoexcited electrons and holes. After releasing the strain and subsequently applying 8 V voltage, the strain-induced slip planes and lattice defects could be electrically healed and thus disappear completely. As a result, the conductance of SnO_2 microrod returns back to its original state. Here, it is worth mentioning that the slight difference between the current after "reset" process and the dark current (see Figure S2 in the Supporting Information) should be associated with the thermal effect, as well as some residual photogenerated carriers. Notably, according to the previous reports, the course of PPC can be effectively accelerated by the application of a high-voltage pulse.[14,17] However, the PPC was only changed a little by applying a voltage pulse (8 V) in our simple system (see Figure S3 in the Supporting Information). Thus, the removal of PPC in SnO_2 microrod cannot be attributed to the application of 8 V voltage.

Table 1. Comparison of the dark current, internal gain, and recovery time between the present SnO_2 single microrod photodetector and the previous reports for other micro/nanostructured SnO_2 photodetectors.

Photodetector	Dark current	Gain	Recovery time	Ref.
SnO_2 monolayer nanofilm	60–90 μA/1 V	–	>50 s	[19]
SnO_2 nanowire array	77 μA/12 V	–	>150 s	[32]
Sb-doped SnO_2 nanowire	2 pA/1 V	3000	≈1 s	[18]
SnO_2 nanowire	19.4 nA/1 V	1.32×10^7	>50 s	[23]
SnO_2 nanowire array	2 pA/1 V	1.32×10^6	10 s	[33]
SnO_2 nanowire	2 nA/0.1 V	10^4–10^7	–	[34]
SnO_2 microrod	13 μA/1 V	1.5×10^9	<1 s	This work

Figure 7a shows the responsivity of the SnO_2 single microrod photodetector at different wavelengths with the applied voltage of 2 V. The photoresponse exhibits a significant increase at around 350 nm, which is close to the band gap energy of SnO_2. The responsivity R is determined as $R_\lambda = I_{\text{Photocurrent}}/(SP_\lambda)$, where S is the effective illuminated area, P_λ is the incident light intensity. In Figure 7a, the responsivity of the device increases by more than six orders of magnitude with the wavelength decreasing from 600 nm to 230 nm. At 250 nm, the responsivity could reach as high as $\approx 3 \times 10^8$ A W^{-1}. According to previous reports, the responsivity (R_λ) of a photoconductor could be also calculated using the following equation[3]

$$R_\lambda = \frac{q\lambda\eta G}{hc} \tag{4}$$

where q is the elementary charge, λ is the wavelength, η is the quantum efficiency, G is the internal gain, h is the Planck constant, and c is the light velocity. Thus, the internal gain of the SnO_2 photoconductor can be calculated to be $\approx 1.5 \times 10^9$ at 250 nm (assuming the quantum efficiency is 100%). This value is much higher than that of other SnO_2 photodetectors reported previously (see Table 1).[18,19,23,32–34] Notably, the SnO_2 microrod photodetector shows an obvious response to the visible light, which should be associated with the deep level defects in microrod. Figure 7b shows the time-dependent photoresponse of the SnO_2 microrod. This was measured by periodically turning on and off the 260 nm light with different intensities. As shown in the middle of Figure 7b, the photoresponse to the on/off light cycles shows poor reproducibility due to the giant PPC effect. Concretely speaking, after the first cycle of UV light on/off (0.03 μW cm^{-2}), the current decays very slowly and does not recover to the initial value, and then increases slightly after two further cycles with the same light intensity. In the fourth and fifth cycles, the light intensity is increased to 0.05 and 0.07 μW cm^{-2}, respectively, and the current increases correspondly. After that, the device does not show any response to the UV light with the intensity of 0.03 μW cm^{-2} in the seventh

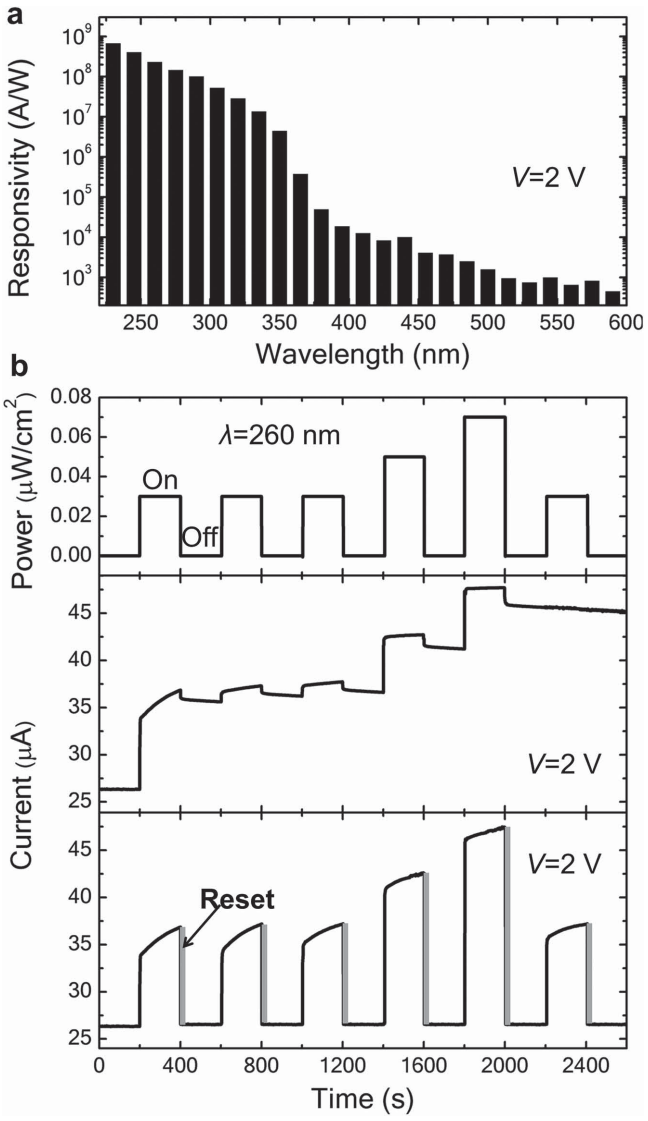

Figure 7. a) The photoresponse spectrum of the SnO_2 single microrod photodetector at 23 °C with the applied voltage of 2 V. b) Time-dependent photocurrent response measured in dry air at a bias voltage of 2 V under 260 nm illumination with different light intensities. Good reproducibility can be obtained after the reset process.

cycle. In contrast, the "reset" process after turning off the light could lead to a stable and reproducible photoresponse as shown in the bottom of Figure 7b. In addition, the response speed of our device is also very quick and the 10–90% rise time is in the range of 1–80 s for different illumination intensities. This result indicates that our SnO_2 microrod photoconductors with high internal gain can be used to detect the high-frequency modulation of UV light with the high signal-to-noise ratio.

3. Conclusion

To summarize, we have demonstrated the novel potential of single SnO_2 microrod UV photoconductor on the flexible substrate. The device shows excellent UV light selectivity and an ultrahigh internal gain ($\approx 1.5 \times 10^9$), which is much higher than that of the previously reported SnO_2 UV photodetectors. However, the SnO_2 microrod photoconductor suffers from the giant PPC effect and its recovery time is on the scale of days. Interestingly, the recovery time of the SnO_2 device can be reduced to less than 1 s by a novel "reset" process: bending and straightening the microrod and subsequently applying a voltage pulse. The elimination of PPC effect by this "reset" process can be explained as follows. 1) Free electrons can be trapped by the bending-strain-induced defects. 2) Applying a voltage pulse could electrically heal the strain-induced defects. This process could almost completely remove residual photogenerated carriers (PPC effect) and then the conductance of SnO_2 microrod returns back to its original dark value. The key mechanism is the efficient control of the defects in SnO_2 by the above "reset" process. Our findings in this work demonstrate a novel and feasible method for realizing SnO_2 microrod UV photoconductor with both ultrahigh gain and relatively quick response speed. Mechanical stress to microrods can be applied at high frequency using piezoelectric devices and small actuators; then, a SnO_2 microrod photoconductor works at high frequency. These SnO_2 devices are very suitable for use in the fields of flame sensing, pollution monitoring, and high voltage arc discharge monitoring.

4. Experimental Section

Synthesis and Characterization of SnO_2 Microrods: SnO_2 microrods were grown on the Si substrate by a typical double-tube chemical vapor deposition (CVD) system.[28] A mixture of highly pure (99.999%) SnO_2 powder (0.5 g) and (99.999%) graphite powder (0.5 g) was used as the source. The source was placed in a ceramic boat, which was put at the sealed end of a small quartz tube.[28] The Si substrate was placed at the open end of the quartz tube. The furnace was heated to 200 °C in a vacuum to remove the water and adsorption gas in the source for 10 min. After that, the temperature was increased to 990 °C with a mixed gas flow as the carrier gas (96% Ar + 4% O_2) with a pressure of 9×10^2 Pa. The furnance was kept at this temerature for 60 min and SnO_2 microrods were formed on the surface of Si substrate. The phase and structure of the SnO_2 microrods were identified by a Rigaku AFC7R X-ray diffractometer using Mo Kα radiation (λ = 0.071073 nm) and a transmission electron microscopy (TEM). The morphology and composition of the products were characterized by a field-emission scanning electron microscopy (FESEM, Hitachi S-4800) equipped with an X-ray energy-dispersive spectrometer (EDX).

Fabrication of Single SnO_2 Microrod UV Photoconductors: SnO_2 microrods were collected from the Si substrate. To fabricate microrod devices, the microrods on the Si substrate were first transferred onto a flexible Kapton substrate. Au electrodes were then deposited tightly on SnO_2 microrod and Kapton substrate by a thermal evaporation system using a mask. The electric properties of the device were measured using a picoammeter (Keithley, model 6458). The photoresponse properties were recorded by using a xenon lamp (500 W).

Supporting Information

Supporting Information is available from the Wiley Online Library or from the author.

Acknowledgements

This work was supported in part by the World Premier International Research Center (WPI) Initiative on Materials Nanoarchitectonics, MEXT, Japan, the National Natural Science Foundation of China under

Grant No. 61475153, and in part by the 100 Talents Program of the Chinese Academy of Sciences.

Received: January 19, 2015
Revised: March 20, 2015
Published online: April 13, 2015

[1] H. Kind, H. Yan, B. Messer, M. Law, P. Yang, *Adv. Mater.* **2002**, *14*, 158.
[2] F. Guo, B. Yang, Y. Yuan, Z. Xiao, Q. Dong, Y. Bi, J. Huang, *Nat. Nanotechnol.* **2012**, *7*, 798.
[3] M. Razeghi, A. Rogalski, *J. Appl. Phys.* **1996**, *79*, 7433.
[4] C. Soci, A. Zhang, B. Xiang, S. A. Dayeh, D. P. R. Aplin, J. Park, X. Y. Bao, Y. H. Lo, D. Wang, *Nano Lett.* **2007**, *7*, 1003.
[5] Y.-Q. Bie, Z.-M. Liao, H.-Z. Zhang, G.-R. Li, Y.-B. Zhou, J. Xu, Z.-X. Qin, L. Dai, D.-P. Yu, *Adv. Mater.* **2011**, *23*, 649.
[6] Q. Chen, J. W. Yang, A. Osinsky, S. Gangopadhyay, B. Lim, M. Z. Anwar, M. Asif Khan, D. Kuksenkov, H. Temkin, *Appl. Phys. Lett.* **1997**, *70*, 2277.
[7] E. Monroy, F. Omnes, F. Calle, *Semicond. Sci. Technol.* **2003**, *18*, R33.
[8] X. Fang, S. Xiong, T. Zhai, Y. Bando, M. Liao, U. K. Gautam, Y. Koide, X. Zhang, Y. Qian, D. Golberg, *Adv. Mater.* **2009**, *21*, 5016.
[9] G. Konstantatos, I. Howard, A. Fischer, S. Hoogland, J. Clifford, E. Klem, L. Levina, E. H. Sargent, *Nature* **2006**, *442*, 180.
[10] W. Xing, S.-C. Kung, W. E. van der Veer, W. Yan, T. Ayvazian, J. Y. Kim, R. M. Penner, *ACS Nano* **2012**, *6*, 5627.
[11] S. Lany, A. Zunger, *Phys. Rev. B: Condens. Matter* **2005**, *72*, 035215.
[12] C. H. Liu, J. I. Pankove, *Appl. Phys. Lett.* **1997**, *70*, 1983.
[13] P. Feng, I. Mönch, S. Harazim, G. Huang, Y. Mei, O. G. Schmidt, *Nano Lett.* **2009**, *9*, 3453.
[14] J. Xu, D. You, Y. Tang, Y. Kang, X. Li, H. Gong, *Appl. Phys. Lett.* **2006**, *88*, 072106.
[15] S. Jeon, S.-E. Ahn, I. Song, C. J. Kim, U.-I. Chung, E. Lee, I. Yoo, A. Nathan, S. Lee, J. Robertson, K. Kim, *Nat. Mater.* **2012**, *11*, 301.
[16] Y. Wang, Z. Liao, G. She, L. Mu, D. Chen, W. Shi, *Appl. Phys. Lett.* **2011**, *98*, 203108.
[17] Q. Hou, X. Wang, H. Xiao, C. Wang, C. Yang, H. Yin, Q. Deng, J. Li, Z. Wang, X. Hou, *Appl. Phys. Lett.* **2011**, *98*, 102104.
[18] Q. Wan, E. Dattoli, W. Lu, *Small* **2008**, *4*, 451.
[19] H. Chen, L. Hu, X. Fang, L. Wu, *Adv. Funct. Mater.* **2012**, *22*, 1229.
[20] Y. Wang, X. Jiang, Y. Xia, *J. Am. Chem. Soc.* **2003**, *125*, 16176.
[21] M. Law, H. Kind, B. Messer, F. Kim, P. Yang, *Angew. Chem.* **2002**, *114*, 2511.
[22] K. Liu, M. Sakurai, M. Aono, *Small* **2012**, *8*, 3599.
[23] L. Hu, J. Yan, M. Liao, L. Wu, X. Fang, *Small* **2011**, *7*, 1012.
[24] C.-H. Lin, R.-S. Chen, T.-T. Chen, H.-Y. Chen, Y.-F. Chen, K.-H. Chen, Y.-C. Chen, *Appl. Phys. Lett.* **2008**, *93*, 112115.
[25] S. Mathur, S. Barth, H. Shen, J.-C. Pyun, U. Werner, *Small* **2005**, *1*, 713.
[26] Y. Muraoka, N. Tkubo, Z. Hiroi, *J. Appl. Phys.* **2009**, *105*, 103702.
[27] E. R. Viana, J. C. Gonzalez, G. M. Ribeiro, A. G. de Oliveira, *J. Phys. Chem. C* **2013**, *117*, 7844.
[28] K. Liu, M. Sakurai, M. Aono, *ACS Nano* **2012**, *6*, 7209.
[29] M. Sakurai, K. Liu, M. Aono, *Appl. Phys. Express* **2014**, *7*, 031101.
[30] J. E. Dominguez, L. Fu, X. Q. Pan, *Appl. Phys. Lett.* **2002**, *81*, 5168.
[31] A. Dissanayake, M. Elahi, H. X. Jiang, J. Y. Lin, *Phys. Rev. B: Condens. Matter* **1992**, *45*, 13996.
[32] J.-M. Wu, C.-H. Kuo, *Thin Solid Films* **2009**, *517*, 3870.
[33] D. Kim, G. Shin, J. Yoon, D. Jang, S.-J. Lee, G. Zi, J. S. Ha, *Nanotechnology* **2013**, *24*, 315502.
[34] M.-L. Lu, T.-M. Weng, J.-Y. Chen, Y.-F. Chen, *NPG Asia Mater.* **2012**, *4*, e26.